CHAPTER-6

GLOBAL PULSATIONAL MODE FLUCTUATIONS IN INHOMOGENEOUS DUST MOLECULAR CLOUD WITH DUST-CHARGE VARIATION

Abstract: *A new evolutionary analytic model for investigating the nonlinear gravito-electrostatic waves in a self-gravitating inhomogeneous planar collisional dust molecular cloud (DMC) on the Jeans scales of space and time is constructed. It includes dust-charge variation and weak but finite inertia of the thermal electrons and ions on the stability time scale. All the equilibrium gradients and inhomogeneities arising from the dynamics of the plasma constituents are considered. Thus, any conventional homogenization assumption, like the Jeans swindle, for mathematical simplification is avoided to depict the actual scenario. By standard inhomogeneous multiple scaling techniques, it is methodologically shown that the fluctuations are collectively governed by a unique gravito-electrostatically coupled pair of driven Korteweg-de Vries (d-KdV) equations with new gradient-driven variable coefficients and self-consistent linear driving sources. A numerical analysis portrays the co-existing eigenmode excitations as oscillatory shock- and soliton-like structures. In addition, depending on the explicit regions of the varied plasma parameter space and inhomogeneities, a new shape-transition from soliton to shock and vice-versa is noticed. The exact results obtained can rigorously be applied to explain diverse multispace satellite observations and predictions made by others in space and astrophysical environments.*

6.1 INTRODUCTION

The presence of the dust grains in the space and astrophysical environments have attracted a great deal of attention due to their ubiquitous nature. They are not uniformly distributed in the interstellar media, rather they are accumulated in the molecular clouds [1-3]. Various physical properties of the dust grains in the interstellar clouds are elaborately discussed in chapter 1. The propagation of various waves and instabilities in such astrophysical dust molecular clouds (DMCs) have received much attention because of their vital role in understanding various fundamental processes in the formation progressions of stars, asteroid zones, planetary rings, and other galactic objects [1-4].

The dust grains of the interstellar media get electrically charged due to various competing phenomena assisted by the electron and ion capture in background plasma environments [1-3]. The grains also lose charges by processes like secondary emission, photo-emission of electrons, and so forth. So, the grain charge $q_d = Z_d e$ indeed may fluctuate from $\pm 1e$ and 0 in cold (dark) cloud at $T < 30$ K, and $q_d > 100e$ in the HII region at $T \sim 10^4$ K [1-5]. Thus, the grain-charge behaves as a dynamical variable owing mainly due to the attachment of the electrons and ions to the grain-surface randomly. It has been found that the presence of the grains with fluctuating charge in astrophysical environments not only modifies existing plasma wave spectrum [3, 5-8], but also give rise to different low-frequency waves and oscillations, both with [3, 5-6] and without [7-8] self-gravity. The modification of the wave spectra occurs due to the reduction in number density of the plasma thermal species; and due to subsequent introduction of new time scales. The existence of such modified eigenmodes in diverse situations has been studied theoretically [5-8] as well as experimentally [9]. To name a few, *Rao et al.* have first theoretically predicted the existence of low-frequency nonlinear eigenmodes in unmagnetized dust-electron-ion plasma, where, the charged grains provide the inertia; and the pressure of the inertialess electrons and ions provides the corresponding restoring force triggering longitudinal plasma sound modes [10].

The presence of the massive grains in the interstellar DMC, between and around comets and other astrophysical objects, has been known for long time from remote astronomical and satellite observations [1-4, 9]. As the massive grains are present in astrophysical plasmas, the gravitational effects become significant. For plasmas with medium-sized electrically charged grains, both the self-gravitational and electrostatic repulsive effects balance each other [5, 11]. So, in interstellar DMC, there are gravito-electrostatic coupling processes responsible for the development of any bounded structure of the Jeans-scale size. When the self-gravitational interaction with relative streaming between plasma and the dust component is included, the Jeans-type instabilities are naturally excited. As a result, different nonlinear eigenmodes in the form of shock, solitons, vortices, etc., evolve, which help in explaining the basic physics of stars, planets, and other galactic structure formation-evolution processes [3-4, 11-12].

There are different models to analyze the propagation of various low-frequency eigenmodes in diverse plasma environments. Most of the investigations have predicted that the dynamical behavior of the eigenmodes is described by the Korteweg–de Vries (KdV) equation as long as the plasma equilibrium is homogeneous [7, 11]. Recently, *Mandal et al.* have studied the

nonlinear propagation of low-frequency shock waves in three-component unmagnetized dusty plasma consisting of nonextensive electrons, Maxwellian ions, and arbitrarily charged mobile dust grains in relevance to space and laboratory plasmas [13]. They have found that the presence of *q*-nonextensive electrons and ions can change the nonlinear behavior of shock wave [13]. In reality, due to the equilibrium density gradients and fluctuations, DMCs are also highly inhomogeneous; and equilibrium plasma variables evolve with both space and time [1-4, 12, 14]. But, so far is seen, little work has been carried out to study the full nonlinear eigenmodes in such realistic spatiotemporally inhomogeneous configurations [14-15]. However, nonlinear gravito-electrostatic disturbances in self-gravitating inhomogeneous collisional astrophysical plasma with the weakly inertial thermal species are yet to be understood. Although weak but finite in presence of the massive dust grains, the thermal species might have some dominant roles to affect the excitation and evolution of the normal modes in wide-spatially extended systems in different realistic situations too as proposed in laboratory scale observations [16] as well.

The work of this chapter is motivated by developing the curiosity of understanding the evolutionary dynamics of eigenmode structures excitable in a planar (1-D) self-gravitating inhomogeneous cloud including all the realistic agencies in an external field-free quasi-neutral configuration on the Jeans scale. The key stimulus is to characterize the eigenmodes in presence of the thermal inertia of the cloud, dust-charge fluctuation, various collisional effects, and all the spatiotemporally evolving equilibrium plasma parameters. We adopt a standard methodology of inhomogeneous multiple scaling techniques [17] around a justifiable inhomogeneous gravito-electrostatic equilibrium over the basic derived cloud structure equations. It is found that both the nonlinear electrostatic and self-gravitational fluctuations dynamically evolve like a gravito-electrostatically coupled driven Korteweg-de Vries (*d*-KdV) equations with self-consistent linear sources. A detailed numerical analysis as initial value problems by the fourth-order Runge-Kutta method (stationary) and finite-difference method (spatiotemporal) under some judicious plasma multi-parameter variation is carried out for their micro-dynamics characterization. The fluctuation structures in the astrophysical charge-varying collisional grainy plasma appear mainly in the unique form of oscillatory shocks and solitary spectral patterns [6, 8-9, 12, 14-15], which are subsequently shown to undergo some newer transitions in between the two distinct classes of the spectral patterns in realistic parameter regime. Lastly, this chapter concentrates to discuss the main significance of such eigenmode structures lying in the diverse areas of cloud physics, space

science, and modern astrophysics because of their crucial role played in understanding self-gravitational collapse, formation-evolution of interstellar structure, star formation, and galactic composition and its evolution, etc., as widely explained elsewhere too [12, 15, 18-20].

6.2 PHYSICAL MODEL

A four-component simplified planar self-gravitating DMC is considered under quasi-neutral hydrodynamic inhomogeneous equilibrium configuration. On the astrophysical scales, the plasma bipolar thermal constituents are the thermal electrons, and singly ionized positive ions; and the inertial spherical micron-sized neutral (nonpolar) dust grains, and negatively charged dust grains.

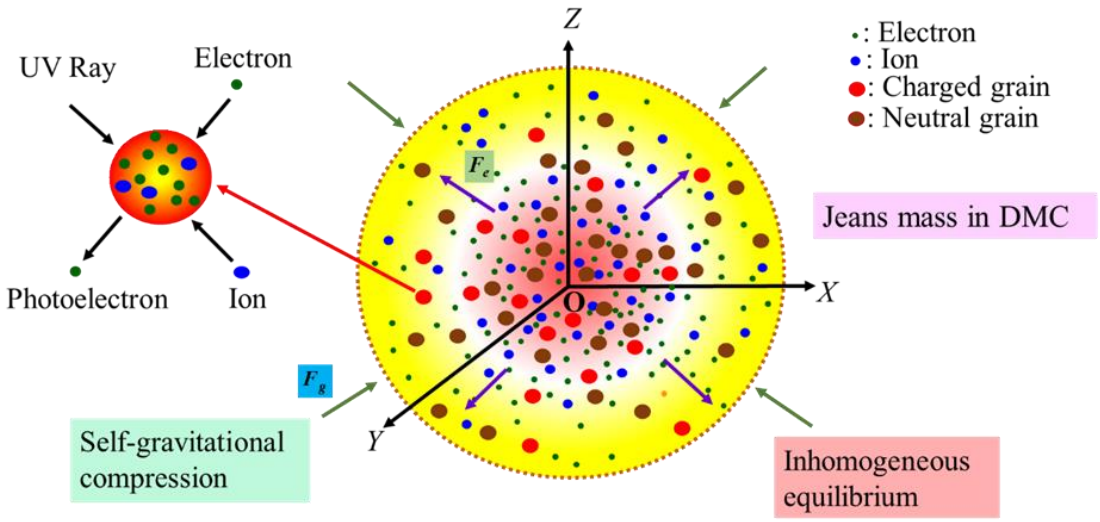

Figure 6.1 *Cartoon showing inhomogeneous, partially-charged DMC adopted in our investigation without any Jeans swindle included. The charging of the grains due to electron, ion bombardments, ultraviolet radiation and photoelectric emission mechanisms is highlighted.*

The assumed planar (1-D) geometry may be equivalent to a spherical symmetry (with infinitely large radius of curvature), wherein, the fluctuations propagate in radial direction only. The dust flow convections, collisional effects, grain-charge fluctuations, and equilibrium gradients of relevant cloud parameters are all taken into account in presence of the lowest-order inertial correction of the thermal species. Since, the model equilibrium is inhomogeneous in nature, so it avoids the Jeans swindle approximation [21-22]. The dynamics of the heavier neutral grains is merely governed by the Newtonian self-gravitational forces, and that of the charged species is

controlled by the effective combination of the Columbic electrostatic and Newtonian gravitational forces. The self-gravitational and electrostatic forces may become commensurable for the grains with high charge-to-mass ratio. A bulk uniform flow is assumed to pre-exist in the hydrodynamic inhomogeneous equilibrium. Figure 6.1 shows the cartoon of a partially-ionized, inhomogeneous, self-gravitating DMC with dust-charge fluctuations.

This may be pertinent to add further that the equilibrium is inhomogeneous due to diverse spatiotemporal gradients of all the relevant dependent plasma parameters with high-frequency (~1 MHz) dust-charge fluctuation. The strength of the electric forces developed due to space-charge polarization effects (local charge imbalance) are taken to be too weak to excite higher order contributions of various harmonics on the Jeans scale, thereby validating our underlying assumption of weak nonlinearity. The existence of a micro-Gauss ($\sim 10^{-6}$ G) magnetic field in interstellar inhomogeneous DMC is well known [21]. The electrically charged grain will gyrate around the magnetic field. Here, for the grains of $m_d \sim 10^{-9}$ kg and $q_d \sim 100e$, the gyration period is estimated as $\sim 10^{10}$ years. This period is as large as the age of our Galaxy ($\sim 10^{10}$ years). Therefore, we may neglect the effect of magnetic field on the constituents. For further simplicity, we ignore the presence of dust-rotation, viscosity, circulation, dust-size distribution, etc.

6.3 BASIC GOVERNING EQUATIONS

The inhomogeneous hydrodynamic equilibrium of the proposed model is visualized as a quasi-static distribution of the multi-fluid constituent particles having both the Newtonian and Coulombic properties. We apply the lowest-order inertial correction [16] of the thermal species in the nonlinear gravito-electrostatic eigenmode analysis of the collisional inhomogeneous DMC. This is incorporated through the modified Boltzmann distributions on the Jeans scale. A standard normalization procedure [5] of the relevant astrophysical parameters is adopted. The modified Boltzmann distributions considering weak but finite inertia of the thermal electrons and the ions in normalized form are directly presented as,

$$N_e = N_{eo} \exp\left[\left(\Phi - \Phi_o\right) - \left(\frac{m_e}{m_d} \right)^{1/2} F_{edc} \xi_e \right], \text{ and} \tag{6.1}$$

$$N_i = N_{io} \exp\left[-\left(\Phi - \Phi_o\right) - \left(\frac{m_i}{m_d} \right)^{1/2} F_{idc} \xi_i \right]. \tag{6.2}$$

Here, F_{edc}, and F_{idc} are the normalized electron-charged dust and ion-charged dust collision frequencies, respectively. Also, ξ_e, and ξ_i denote average electron transit-scale-length and ion transit-scale-length, respectively. It is clearly seen that the presence of the mass-ratios in the above expressions describe the active inertial roles of the thermal species in the relevant response scales. If we consider m_e/m_d, $m_i/m_d \to 0$ for the inertialess electrons and the ions in equations (6.1)-(6.2), they reduce back to the normal inertialess Boltzmann distributions [3, 5]. The main concern here is to examine the effects of these equations in our model fluctuation dynamics. Now, the normalized set of equations governing our model are enlisted as,

$$\frac{\partial N_s}{\partial T} + N_s \frac{\partial M_s}{\partial X} + M_s \frac{\partial N_s}{\partial X} = 0 \text{, and} \tag{6.3}$$

$$\frac{\partial N_s}{\partial X} + \beta N_s \frac{\partial \Phi}{\partial X} + \left(\frac{m_s}{m_d}\right) N_s M_s F_{sdc} = 0 . \tag{6.4}$$

Equations (6.3)-(6.4) governs the dynamics of the electrons ($s = e$, $\beta = -1$), and ions ($s = i$, $\beta = 1$), respectively. Since, we are interested in weakly nonlinear low-frequency fluctuations, we neglect the force-balance inertial term in equation (6.4) as described elsewhere [5]. It is well-known that if the phase speed of the fluctuations is much smaller than the thermal speed of the electrons and ions in a dusty plasma configuration, the dynamics of both the thermal electrons and ions is governed by the Boltzmann population density distribution [23]. In our present analysis, $\phi/\psi \sim m_e/e \sim 10^{-17}$ (in unnormalized form) for the electrons and $\phi/\psi \sim m_i/e \sim 10^{-14}$ (in unnormalized form) for the ions, which are quite small [5]. So, the effect of self-gravity [5] on them is neglected, as clearly seen from equation (6.4). The notation ϕ, and ψ represents the unnormalized electrostatic and self-gravitational potential, respectively. The dynamics of the neutral and charged grains are similarly described by,

$$\frac{\partial N_{dh}}{\partial T} + N_{dh} \frac{\partial M_{dh}}{\partial X} + M_{dh} \frac{\partial N_{dh}}{\partial X} = 0 \text{, and} \tag{6.5}$$

$$\left[\frac{\partial M_{dh}}{\partial T} + M_{dh} \frac{\partial M_{dh}}{\partial X}\right] = -\Omega Q_d \frac{\partial \Phi}{\partial X} - \left(\frac{T_d}{T_p}\right) \frac{1}{N_{dh}} \frac{\partial N_{dh}}{\partial X} - \left(\frac{m_{dh}}{e}\right) \frac{\partial \Psi}{\partial X} - f_h . \tag{6.6}$$

Here, for $h = n$ (neutral dust), one has $\Omega = 0$, and $f_n = F_{nc}\left(M_{dn} - M_{dc}\right)$. Similarly, for $h = c$ (charge dust), we have $\Omega = q_{do}$, and $f_c = F_{cn}\left(M_{dc} - M_{dn}\right)$. The spatial distributions of the electrostatic

potential Φ, and self-gravitational potential Ψ in presence of the weak but finite thermal inertia taken into account are defined by combining electro-gravitational Poisson equations as,

$$\frac{\partial^2 \Phi}{\partial X^2} = \delta_1 \{N_e - \delta_2 N_i + \delta_3 Z_d N_{dc}\}, \tag{6.7}$$

where, $\delta_1 = e^2 n_{eo} / m_{dc}^2 n_{do} G$, $\delta_2 = n_{io}/n_{eo}$ and $\delta_3 = q_{do} n_{dco}/n_{eo}$;

$$\frac{\partial^2 \Psi}{\partial X^2} = \kappa_1 \{N_{dn} + \kappa_2 N_{dc} + \kappa_3 N_e + \kappa_4 N_i\}, \tag{6.8}$$

where, $\kappa_1 = e n_{dno}/m_d n_{do}$, $\kappa_2 = n_{dco}/n_{dno}$, $\kappa_3 = n_{eo} m_e / m_d n_{dno}$, and $\kappa_4 = n_{io} m_i / m_d n_{dno}$. Here, a natural question may arise in the mind of readers. The self-gravitational effects are ignored in the momentum equation (equation (6.4)) of both the thermal electrons and ions with required quantitative justifications, relative to the electrostatic influences. But, in isolation, the weak but finite inertia is assumed to contribute to the net self-gravitational potential distribution (equation (6.8)), although it is much smaller in comparison with that by the grains. Thus, we introduce a weak but finite self-gravitational effect in the dynamics of the electrons and ions in our model on the basis of the calculated relative strength of the gravito-electrostatic coupling of the thermal species in isolation. We consider inhomogeneous material distribution of the self-gravitational infinitely large DMC with the inhomogeneous equilibrium itself spatiotemporally evolving. So, it avoids the Jeans swindle by which the inhomogeneous self-gravitating equilibrium is initially considered as 'homogeneous' for mathematical simplicity [21-22]. Lastly, the charge dynamic equation for the charge-fluctuated grain dynamics is given by,

$$\frac{\partial Q_d}{\partial T} + M_{dc} \frac{\partial Q_d}{\partial X} = \frac{e}{q_{do}} \left(\frac{n_{eo}}{n_{do}}\right) F_{ed} \left[\left\{ N_e - \left(\frac{n_{io}}{n_{eo}}\right) \left(\frac{F_{id}}{F_{ed}}\right) N_i \right\} - \left(1 + \frac{n_{io}}{n_{eo}} \frac{F_{id}}{F_{ed}}\right) \right]. \tag{6.9}$$

In the above normalized set of equations, the notations m_e, m_i, m_{dn} and m_{dc} ($m_{dn} \sim m_{dc} \approx m_d$) are mass of each electron, ion, neutral and charged dust grains with temperature $T_e \sim T_i = T_p >> T_{dn} \sim T_{dc} = T_d$, respectively. The equilibrium dust density is $n_{do} = n_{dco} + n_{dno}$. The independent coordinates like position X and time T are normalized by the Jeans length λ_J and Jeans time ω_J^{-1} scales, respectively. The parameters M_e, M_i, M_{dn}, and M_{dc} represent the flow velocities of the electrons, ions, neutral grains and charged grains normalized by the dust sound phase speed C_{SS} each. Moreover, N_e, N_i, N_{dn}, and N_{dc} are the population densities of the electrons, ions,

neutral grains and charged grains normalized by their equilibrium densities n_{eo}, n_{io}, n_{dno}, and n_{dco}, respectively. Both the electrostatic potential Φ and self-gravitational potential Ψ are normalized by the same electron thermal potential T_P/e so as to compare their fluctuation levels on a common equivalent reference. The grain charge Q_d is normalized by the equilibrium grain charge q_{do}. Lastly, the symbols F_{edc}, F_{ed}, F_{idc}, F_{id}, F_{nc}, and F_{cn} are the collision frequencies of the electrons and charged dust grains; electrons and dust grains; ions and charged dust grains; ions and dust grains; neutral and charged dust grains; and finally, charged and neutral dust grains; respectively, each normalized by the Jeans frequency ω_J.

6.4. DERIVATION OF NONLINEAR EQUATIONS

We apply a standard methodology of inhomogeneous multiple scaling techniques [14, 17] over the coupled set of equations (6.1)-(6.9). The dependent physical variables describing the coupled system are expanded nonlinearly around the equilibrium (in $\in$-powers) as follows,

$$\begin{bmatrix} N_s \\ N_{dh} \\ M_s \\ M_{dh} \\ \Phi \\ \Psi \\ Q_d \end{bmatrix} = \begin{bmatrix} N_{so}(X) \\ N_{dho}(X) \\ M_{so}(X) \\ M_{dho}(X) \\ \Phi_o(X) \\ \Psi_o(X) \\ Q_{do}(X) \end{bmatrix} + \in \begin{bmatrix} N_{s1}(X,T) \\ N_{dh1}(X,T) \\ M_{s1}(X,T) \\ M_{dh1}(X,T) \\ \Phi_1(X,T) \\ \Psi_1(X,T) \\ Q_{d1}(X,T) \end{bmatrix} + \in^2 \begin{bmatrix} N_{s2}(X,T) \\ N_{dh2}(X,T) \\ M_{s2}(X,T) \\ M_{dh2}(X,T) \\ \Phi_2(X,T) \\ \Psi_2(X,T) \\ Q_{d2}(X,T) \end{bmatrix} + \cdots\cdots \qquad (6.10)$$

The independent variables with all usual notations are stretched into a new space defined by the transformations [17] as $\xi = \in^{1/2} (\mu X - T)$, and $\eta = \in^{3/2} X$, where $\mu = 1/\lambda_o$, and λ_o is the phase velocity of the fluctuations (normalized by C_{SS}), and $\in$ is a minor parameter characterizing the strength of nonlinearity and dispersion. We substitute equation (6.10) in equations (6.1)-(6.9) for order-by-order analyses and derived the coupled set of nonlinear equations governing the gravito-electrostatic fluctuations of the inhomogeneous DMC.

6.4.1 Derivation of Electrostatic *d*-KdV Equation

To study the electrostatic fluctuation dynamics of the inhomogeneous DMC, we derived electrostatic *d*-KdV equation (in terms of Φ_1) by applying the systematic methodology of

elimination and simplification after the order-by-order analyses of the equations (6.1)-(6.9). The derived *d*-KdV equation is expressed as,

$$\frac{\partial \Phi_1}{\partial \eta} + A_1 \Phi_1 \frac{\partial \Phi_1}{\partial \xi} + A_2 \frac{\partial^3 \Phi_1}{\partial \xi^3} + A_3 \frac{\partial \Phi_1}{\partial \xi} = S_{eo}. \tag{6.11}$$

Here, $S_{eo} = \left(A_4 \Phi_1 + A_5\right)$ acts as a self-consistent linear source in the evolution of the fluctuation dynamics due to various equilibrium inhomogeneities. The involved coefficients are $A_1 = \alpha_2/\alpha_1$, $A_2 = \alpha_3/\alpha_1$, $A_3 = \alpha_4/\alpha_1$, $A_4 = \alpha_5/\alpha_1$ and $A_5 = \alpha_6/\alpha_1$, where,

$$\alpha_1 = \frac{1}{\left(1-\mu M_{dco}\right)}\left\{\frac{e n_{eo} N_{eo}\left(1-\mu M_{dco}\right)}{\mu}\left(1-\frac{F_{ed}}{F_{id}}\right) + q_{do}^2 N_{dco}\left(1+\mu M_{dco}\right)\frac{\partial Q_{dco}}{\partial M_{dco}} - M_{dco} e\left(n_{io} N_{io} a_2 - n_{eo} N_{eo} a_1\right)\left(\frac{\partial Q_{dco}}{\partial X}\right)^{-1}\right\}, \tag{6.12}$$

$$\alpha_2 = a_1 N_{io} e\left(1-\frac{F_{ed}}{F_{id}}\right) - \frac{\mu e\left(n_{io} N_{io} a_2 - n_{eo} N_{eo} a_1\right)}{\left(1-\mu M_{dco}\right) Q_{do}}\left[\left\{\frac{\mu e\left(n_{io} N_{io} a_2 - n_{eo} N_{eo} a_1\right) n_{dco}^2}{\left(1-\mu M_{dco}\right) Q_{do} q_{do} N_{dco}} + \frac{q_{do} Q_{do} \mu}{n_{dco}\left(1-\mu M_{dco}\right)}\right\} + \left\{\frac{e n_{dno}\left(1-\mu M_{dco}\right)^2}{\mu N_{dco}} + \frac{e\mu n_{dco}}{N_{dno} n_{dco}}\right\}\left\{\frac{\left(n_{io} N_{io} a_2 - n_{eo} N_{eo} a_1\right) n_{dco}^2}{\left(1-\mu M_{dco}\right) Q_{do} q_{do}}\right\} + \frac{\mu N_{io} a_2 n_{io}}{\left(1-\mu M_{dco}\right) N_{dno} n_{dco} n_{dno}}\left(\frac{m_e F_{id}}{m_d F_{ed}} + \frac{m_i}{m_d}\right)\right], \tag{6.13}$$

$$\alpha_3 = \frac{m_d^2 n_{do} G \mu^2}{e}, \tag{6.14}$$

$$\alpha_4 = -\frac{e M_{dco} \tau_{cf}\left(n_{io} N_{io} a_2 - n_{eo} N_{eo} a_1\right)}{Q_{do}}\frac{\partial Q_{do}}{\partial \eta} - \frac{q_{do} n_{dco} \mu N_{dco}}{\left(1-\mu M_{dco}\right)}\left\{\frac{\mu M_{dco} \tau_{cf}\left(1+\mu M_{dco}\right)}{\left(1-\mu M_{dco}\right)}\frac{\partial M_{dco}}{\partial \eta} - \frac{M_{dco} \tau_{cf}}{Q_{do}}\frac{\partial Q_{do}}{\partial \eta}\right\}\left[\left\{\frac{\mu e\left(n_{io} N_{io} a_2 - n_{eo} N_{eo} a_1\right) n_{dco}^2}{\left(1-\mu M_{dco}\right) Q_{do} q_{do} N_{dco}} + \frac{q_{do} Q_{do} \mu}{n_{dco}\left(1-\mu M_{dco}\right)}\right\} + \left\{\frac{e\mu n_{dco}}{N_{dno} n_{dco}} + \frac{e n_{dno}\left(1-\mu M_{dco}\right)^2}{\mu N_{dco}}\right\}\left\{\frac{\left(n_{io} N_{io} a_2 - n_{eo} N_{eo} a_1\right) n_{dco}^2}{\left(1-\mu M_{dco}\right) Q_{do} q_{do}}\right\} + \frac{\mu N_{io} a_2 n_{io}}{\left(1-\mu M_{dco}\right) N_{dno} n_{dco} n_{dno}}\left(\frac{m_e F_{id}}{m_d F_{ed}} + \frac{m_i}{m_d}\right)\right], \tag{6.15}$$

$$\alpha_5 = -\frac{a_1 e}{\mu}\left\{\frac{\partial N_{eo}}{\partial \eta} - N_{eo}\frac{\partial \Phi_o}{\partial \eta}\right\}\left(\frac{F_{id}}{F_{ed}} - 1\right) + \frac{e\left(n_{io} N_{io} a_2 - n_{eo} N_{eo} a_1\right)}{Q_{do}}\left(\frac{\partial Q_{do}}{\partial \eta}\right) + \frac{M_{dco}}{e\left(1-\mu M_{dco}\right)}\left(\frac{\partial Q_{do}}{\partial \eta}\right)\left(n_{io} a_2 \frac{\partial N_{io}}{\partial \eta} - n_{eo} a_1 \frac{\partial N_{eo}}{\partial \eta}\right) + \frac{e\left(n_{io} N_{io} a_2 - n_{eo} N_{eo} a_1\right)}{Q_{do}\left(1-\mu M_{dco}\right)}\left[\frac{\partial M_{dco}}{\partial \eta} + \frac{\partial N_{dco}}{\partial \eta} + \frac{q_{do} Q_{do}}{\left(1-\mu M_{dco}\right)}\frac{\partial \Phi_o}{\partial \eta} + \frac{M_{dco}}{\left(1-\mu M_{dco}\right)}\frac{\partial M_{dco}}{\partial \eta}\left(1-\frac{T_d}{T_P}\right) + \frac{T_d}{T_P N_{dco}\left(1-\mu M_{dco}\right)}\frac{\partial N_{dco}}{\partial \eta}\right.$$

$$-\frac{T_d}{(1-\mu M_{dco})T_P}\frac{\partial N_{dno}}{\partial \eta}-\frac{M_{dco}}{(1-\mu M_{dco})}\frac{\partial Q_{do}}{\partial \eta}\left\{\frac{\mu T_d}{T_P}+\frac{(1-\mu M_{dco})^2}{\mu Q_{do}}+\frac{\mu N_{dco}n_{dco}T_d}{Q_{do}N_{dno}n_{dno}T_P}\right\}$$
$$+\frac{m_d}{e(1-\mu M_{dco})}\left\{\frac{Q_{do}q_{do}N_{dco}}{e(n_{io}N_{io}-n_{eo}N_{eo})}\right\}\frac{\partial \Psi_o}{\partial \eta}-\left(N_{dco}\frac{\partial N_{dco}}{\partial \eta}+M_{dco}\frac{\partial N_{dco}}{\partial \eta}\right)\frac{1}{\mu N_{dco}}\Bigg], \tag{6.16}$$

$$\alpha_6=-2\left\{\frac{q_{do}M_{dco}^2N_{dco}\tau_{cf}}{Q_{do}}\left(\frac{\partial Q_{do}}{\partial \eta}\right)^2\right\}-\frac{q_{do}M_{dco}N_{dco}\tau_{cf}}{(1-\mu M_{dco})}\frac{\partial N_{dco}}{\partial \eta}\frac{\partial Q_{do}}{\partial \eta}+\frac{\partial M_{dco}}{\partial \eta}$$
$$\frac{q_{do}\,\mu M_{dco}\,\tau_{cf}}{(1+\mu M_{dco})(1-\mu M_{dco})}-\frac{q_{do}\,M_{dco}\,\tau_{cf}}{(1-\mu M_{dco})}\left(M_{dco}\frac{\partial N_{dco}}{\partial \eta}-N_{dco}\frac{\partial M_{dco}}{\partial \eta}\right)-$$
$$\frac{q_{do}M_{dco}N_{dco}\tau_{cf}}{Q_{do}(1-\mu M_{dco})}\frac{\partial M_{dco}}{\partial \eta}\frac{\partial Q_{do}}{\partial \eta}+\frac{q_{do}\mu N_{dco}}{(1-\mu M_{dco})}\left\{\frac{\mu M_{dco}\tau_{cf}}{(1+\mu M_{dco})(1-\mu M_{dco})}\right.$$
$$\left.\frac{\partial M_{dco}}{\partial \eta}-\frac{M_{dco}\,\tau_{cf}}{Q_{do}}\frac{\partial Q_{do}}{\partial \eta}\right\}\Bigg[\left\{-\frac{\mu T_d}{\mu T_p}-\frac{n_{dco}(1-\mu M_{dco})^2}{\mu Q_{do}}-\frac{\mu N_{dco}\,n_{dco}T_d}{n_{dno}N_{dno}\,Q_{do}T_p}\right\}\frac{\partial Q_{do}}{\partial \eta}$$
$$\frac{M_{dco}}{(1-\mu M_{dco})}+\frac{m_d}{e(1-\mu M_{dco})}\left\{\frac{Q_{do}q_{do}N_{dco}}{e(n_{io}N_{io}-n_{eo}N_{eo})}-1\right\}\frac{\partial \Psi_o}{\partial \eta}+\frac{\partial N_{dco}}{\partial \eta}$$
$$\frac{T_d}{N_{dco}(1-\mu M_{dco})T_p}+\frac{n_{dno}}{n_{dco}\mu N_{dco}}\left(N_{dco}\frac{\partial M_{dco}}{\partial \eta}+M_{dco}\frac{\partial N_{dco}}{\partial \eta}\right)-\left(M_{dco}\frac{\partial M_{dco}}{\partial \eta}\right.$$
$$\left.+\frac{T_d}{T_p}\frac{\partial N_{dno}}{\partial \eta}\right)\frac{1}{(1-\mu M_{dco})}+\frac{q_{do}Q_{do}}{(1-\mu M_{dco})}\frac{\partial \Phi_o}{\partial \eta}+\frac{M_{dco}}{(1-\mu M_{dco})}\frac{\partial M_{dco}}{\partial \eta}\Bigg], \tag{6.17}$$

$a_1=1-(m_e/m_d)^{1/2}F_{edc}\xi_e$, and $a_2=-1+(m_i/m_d)^{1/2}F_{idc}\xi_i$. (6.18)

6.4.2 Derivation of Self-gravitational *d*-KdV Equation

To study the self-gravitational eigenmodes, we derive *d*-KdV equation (in terms of Ψ_1) by using analogous technique and spade-work over the order-by-order analyses as,

$$\frac{\partial \Psi_1}{\partial \eta}+B_1\Psi_1\frac{\partial \Psi_1}{\partial \xi}+B_2\frac{\partial^3\Psi_1}{\partial \xi^3}+B_3\frac{\partial \Psi_1}{\partial \xi}=S_{go}. \tag{6.19}$$

Here too, $S_{go}=(B_4\Psi_1+B_5)$ acts as a self-consistent linear source in the evolution of self-gravitational fluctuation dynamics due to equilibrium inhomogeneities. The different coefficients are $B_1=\gamma_2/\gamma_1$, $B_2=\gamma_3/\gamma_1$, $B_3=\gamma_4/\gamma_1$, $B_4=\gamma_5/\gamma_1$ and $B_5=\gamma_6/\gamma_1$, where,

$$\gamma_1=\frac{n_{dco}}{n_{dno}\,e\,q_{do}(1+\mu M_{dco})}\left\{\frac{(n_{eo}\,m_e\,a_1\,N_{eo}+n_{io}\,m_i\,a_2\,N_{io})}{(1-\mu M_{dco})}+\frac{n_{eo}\,N_{eo}}{\mu M_{dco}}\left(m_e+m_i\frac{F_{ed}}{F_{id}}\right)\right\}+\frac{m_d(n_{dno}N_{dno}+n_{dco}N_{dco})}{(1-\mu M_{dco})n_{dno}eM_{dco}}, \tag{6.20}$$

$$\gamma_2 = \frac{\mu^3 m_d^2 N_{dno}}{M_{dno} e^2 \left\{ \left(1-\mu M_{dco}\right)^2 - \frac{\mu^2 T_d}{T_p} \right\} \left(1-\mu M_{dco}\right)} + \frac{m_d^2 n_{dco}}{q_{do}^2 n_{dno} e M_{dco}^2} \frac{\partial M_{dco}}{\partial Q_{do}} \left\{ \frac{u\left(n_{io} N_{io} a_2 - n_{eo} N_{eo} a_1\right)}{\left(1-\mu^2 M_{dco}^2\right) Q_{do}} \right.$$
$$\left. + \frac{a_1 N_{eo} n_{eo} n_{dco}}{n_{dno} e\left(1+\mu M_{dco}\right)} \frac{\partial M_{dco}}{\partial Q_{do}} \left(\frac{m_e}{m_d} + \frac{m_i}{m_d} \frac{F_{ed}}{F_{id}} \right) \right\}, \tag{6.21}$$

$$\gamma_3 = \frac{m_d n_{dno} \mu^2}{e}, \tag{6.22}$$

$$\gamma_4 = \left\{ \frac{\mu^3 N_{dno} n_{dno} M_{dco}^2}{\left(1-\mu M_{dco}\right)^2 - \frac{\mu^2 T_d}{T_p}} \frac{\partial M_{dco}}{\partial \eta} log\left(M_{dco} \tau_{cf} \frac{\partial Q_{do}}{\partial \eta} \right) - \frac{\left(n_{eo} m_e a_1 N_{eo} + n_{io} m_i a_2 N_{io}\right)}{M_{dco} n_{dco} m_d} \right\}$$
$$\frac{\mu m_d}{e\left(1-\mu M_{dco}\right)} + \left\{ \frac{\mu\left(n_{io} a_2 N_{io} - n_{eo} a_1 N_{eo}\right)}{Q_{do}\left(1-\mu M_{dno}\right)} + \frac{n_{eo} a_1 N_{eo} n_{dco}}{e n_{dno}\left(1+\mu M_{dno}\right)^3} \frac{\partial M_{dco}}{\partial Q_{do}} \right\} \tag{6.23}$$
$$\frac{\mu m_d M_{dco} n_{dco}}{q_{do}^2} log\left(M_{dco} \tau_{cf} \frac{\partial Q_{do}}{\partial \eta} \right) \frac{\partial M_{dco}}{\partial Q_{do}} \frac{\partial M_{dco}}{\partial \eta},$$

$$\gamma_5 = \frac{m_d}{\left(1-\mu M_{dno}\right) e M_{dno} n_{dno}} \left(n_{dno} \frac{\partial N_{dno}}{\partial \eta} + n_{dco} \frac{\partial N_{dco}}{\partial \eta} \right) - \frac{\left(n_{dno} N_{dno} + n_{dco} N_{dco}\right)}{e M_{dco}^2 \left(1-\mu^2 M_{dno}^2\right)} \frac{\partial M_{dco}}{\partial \eta}$$
$$\frac{m_d\left(1+2\mu M_{dco}\right)}{n_{dno}} + \frac{n_{dco}}{n_{dno} M_{dno} q_{do} e\left(1-\mu^2 M_{dno}^2\right)} \frac{\partial M_{dco}}{\partial \eta} \left\{ \left(n_{eo} m_e a_1 N_{eo} + n_{io} m_i a_2 N_{io}\right) \frac{\partial M_{dco}}{\partial \eta} \right.$$
$$\left. + M_{dno} \left(n_{eo} m_e a_1 \frac{\partial N_{eo}}{\partial \eta} + n_{io} m_i a_2 \frac{\partial N_{io}}{\partial \eta} \right) \right\} - \frac{n_{dco}\left(n_{eo} m_e a_1 N_{eo} + n_{io} m_i a_2 N_{io}\right)}{\left(1-\mu M_{dno}\right) M_{dco}\left(1+\mu M_{dno}\right)^2} \frac{\left(1+2\mu M_{dco}\right)}{n_{dno} e q_{do}}$$
$$\frac{\partial M_{dco}}{\partial \eta} \frac{\partial M_{dco}}{\partial Q_{do}} + \left\{ N_{dno} M_{dno} \frac{\partial M_{dno}}{\partial \eta} + \frac{m_d N_{dno}}{e n_{dno}} \frac{\partial \Psi_o}{\partial \eta} + \frac{T_d}{n_{dno} T_p} \frac{\partial N_{dno}}{\partial \eta} \frac{\left(1-\mu M_{dno}\right)}{\mu} \right.$$
$$\left. + \frac{\partial}{\partial \eta}\left(N_{dno} M_{dno}\right) \right\} \frac{\mu^2 m_d n_{dno}}{\left(1-\mu M_{dno}\right) M_{dno} e \left\{ \left(1-\mu M_{dno}\right)^2 - \frac{\mu^2 T_d}{T_p} \right\}} + \left\{ \frac{e\left(n_{io} N_{io} a_2 - n_{eo} N_{eo} a_1\right) \mu M_{dco}^2}{q_{do}^2 Q_{do}\left(1+\mu M_{dno}\right)^3 \tau_{cf}} \right.$$
$$\left. \frac{\partial M_{dco}}{\partial \eta} \frac{\partial M_{dco}}{\partial Q_{do}} - \frac{N_{eo} M_{dco}}{Q_{do}} \frac{\partial Q_{do}}{\partial \eta} \right\} \frac{m_d \mu n_{dco}}{M_{dno} n_{dco} e\left(1-\mu M_{dno}\right)} + \frac{n_{dco}^2 \mu M_{dco}^2 a_1 n_{eo} N_{eo}}{q_{do}^2 n_{dno} e M_{dno}\left(1+\mu M_{dno}\right)^4 \tau_{cf}} \frac{\partial M_{dco}}{\partial \eta} \tag{6.24}$$
$$\left(m_e + m_i \frac{F_{ed}}{F_{id}} \right) \left(\frac{\partial M_{dco}}{\partial Q_{do}} \right)^2 - \left(m_e + m_i \frac{F_{ed}}{F_{id}} \right) \frac{n_{eo} N_{eo} n_{dco}\left(1+2\mu M_{dco}\right)}{\mu n_{dno} e q_{do} M_{dco}^2 \left(1+\mu M_{dno}\right)^3} \frac{\partial M_{dco}}{\partial \eta} \frac{\partial M_{dco}}{\partial Q_{do}}$$
$$- \frac{n_{dco}}{n_{dno} e M_{dco} q_{do}\left(1+\mu M_{dno}\right)} \frac{\partial M_{dco}}{\partial Q_{do}} \frac{n_{eo} a_1}{\mu} \left(\frac{\partial N_{eo}}{\partial \eta} - N_{eo} \frac{\partial \Phi_o}{\partial \eta} \right) \left(m_e + m_i \frac{F_{ed}}{F_{id}} \right),$$

$$\gamma_6 = \left\{ \frac{\mu^3 N_{dno} n_{dno} M_{dco}^2}{(1-\mu M_{dco})^2 - \frac{\mu^2 T_d}{T_p}} \frac{\partial M_{dco}}{\partial \eta} \log\left(M_{dco} \tau_{cf} \frac{\partial Q_{do}}{\partial \eta} \right) - \frac{(n_{eo} m_e a_1 N_{eo} + n_{io} m_i a_2 N_{io})}{M_{dco} n_{dco} m_d} \right\}$$
$$\frac{\mu m_d}{e(1-\mu M_{dco})} + \left\{ \frac{\mu(n_{io} a_2 N_{io} - n_{eo} a_1 N_{eo})}{Q_{do}(1-\mu M_{dno})} + \frac{n_{eo} a_1 N_{eo} n_{dco}}{e n_{dno}(1+\mu M_{dno})^3} \frac{\partial M_{dco}}{\partial Q_{do}} \right\} \tag{6.25}$$
$$\frac{\mu m_d M_{dco} n_{dco}}{q_{do}^2} \log\left(M_{dco} \tau_{cf} \frac{\partial Q_{do}}{\partial \eta} \right) \frac{\partial M_{dco}}{\partial Q_{do}} \frac{\partial M_{dco}}{\partial \eta}.$$

6.4.3 Stationary Evolution Equations

We look for possible time-stationary structures of the gravito-electrostatic fluctuations. So, we assume that all the variables in equations (6.11)-(6.19) depend only on a single space coordinate $\rho = \eta - \xi$ (commoving frame). Thus, equations (6.11) and (6.19) in stationary form are,

$$\frac{\partial \Phi_1}{\partial \rho} + \frac{A_1}{(A_3 - 1)} \Phi_1 \frac{\partial \Phi_1}{\partial \rho} + \frac{A_2}{(A_3 - 1)} \frac{\partial^3 \Phi_1}{\partial \rho^3} = \frac{(A_4 \Phi_1 + A_5)}{(1 - A_3)}, \text{ and} \tag{6.26}$$

$$\frac{\partial \Psi_1}{\partial \rho} + \frac{B_1}{(B_3 - 1)} \Psi_1 \frac{\partial \Psi_1}{\partial \rho} + \frac{B_2}{(B_3 - 1)} \frac{\partial^3 \Psi_1}{\partial \rho^3} = \frac{(B_4 \Psi_1 + B_5)}{(1 - B_3)}. \tag{6.27}$$

Both the equations are self-consistently coupled amid gravito-electrostatic coupling through the presence of the coefficients A_4, A_5 (for electrostatic) and B_4, B_5 (for self-gravitational), which are driven by inhomogeneous equilibrium gradients in both space and time simultaneously.

6.5 RESULTS AND DISCUSSIONS

It is analytically shown that the lowest-order gravito-electrostatic eigenmode evolutions are expressible by a unique pair of *d*-KdV equations obtained by inhomogeneous multiscale analyses. They are simulated numerically as initial value problems in a time-stationary configuration by the RK-IV method [24]. The time-dependent salient features of their evolutionary dynamics are also analyzed by finite-difference method [24]. The observed numerical results are presented in two subsections: one for the electrostatic, and the other for the self-gravitational fluctuations.

6.5.1 Electrostatic Fluctuations

The electrostatic fluctuations of the cloud is collectively governed by the *d*-KdV equation (6.11). It contains a self-consistent linear driving source term arising due to the weak but finite inertial effect, inhomogeneity, collision, equilibrium flow of thermal species, dust grains and equilibrium

charged-dust distribution. To get the internal microphysics of the fluctuations, the *d*-KdV equation is integrated spatiotemporally by numerical techniques. The time-stationary results are shown in figure 6.2 and time-dependent results are displayed in figure 6.3.

Figure 6.2 portrays spatial profile of the normalized lowest-order perturbed (a) electrostatic potential showing a unique dynamical transition from soliton to oscillatory shock-like structure, (b) electric field, (c) potential curvature, and (d) phase portrait due to multi-parameter variation on the Jeans scale-length. Various lines correspond to Case (1): $m_d = 7.00\times10^{-9}$ kg, $n_{dco} = 5.00\times10^{1}$ m^{-3}, $n_{eo} = 1.00\times10^{3}$ m^{-3}, and $n_{io} = 7.00\times10^{3}$ m^{-3} (blue line), Case (2): $m_d = 6.30\times10^{-9}$ kg, $n_{dco} = 7.33\times10^{1}$ m^{-3}, $n_{eo} = 6.60\times10^{2}$ m^{-3}, and $n_{io} = 7.50\times10^{3}$ m^{-3} (red line), Case (3): $m_d = 5.60\times10^{-9}$ kg, $n_{dco} = 9.66\times10^{1}$ m^{-3}, $n_{eo} = 3.30\times10^{2}$ m^{-3}, and $n_{io} = 8.00\times10^{3}$ m^{-3} (green line), and Case (4): $m_d = 4.90\times10^{-9}$ kg, $n_{dco} = 1.20\times10^{2}$ m^{-3}, $n_{eo} = 1.00\times10^{2}$ m^{-3}, and $n_{io} = 8.50\times10^{3}$ m^{-3} (black line), respectively. Different input initial values used $(N_{eo})_i = 1.00$, $(M_{eo})_i = 1.00\times10^{-1}$, $(\Phi_o)_i = 1.00\times10^{-3}$, $(\Phi_o)_{\rho i} = 1.00\times10^{-7}$, $(N_{io})_i = 1.00$, $(M_{io})_i = 4.00\times10^{-2}$, $(N_{dco})_i = 1.00$, $(M_{dco})_i = 3.00\times10^{-2}$, $(M_{dno})_i = 3.00\times10^{-2}$, $(\Psi_o)_i = 1.00\times10^{-6}$, $(\Psi_o)_{\rho i} = 1.00\times10^{-8}$, $(Q_{do})_i = 1.00$, $(N_{dno})_i = 1.00$, $(\Phi_1)_i = -9.20\times10^{-5}$, $(\Phi_1)_{\rho i} = -1.01\times10^{-4}$, $(\Phi_1)_{\rho\rho i} = 4.01\times10^{-3}$. Different parameters kept fixed are $n_{dno} = 1.00\times10^{-1}$ m^{-3}, $\mu = 1.00\times10^{-2}$, $F_{edc} = 1.10\times10^{2}$, $F_{idc} = 1.00\times10^{2}$, $F_{ed} = 1.343\times10^{2}$, $F_{id} = 2.043\times10^{2}$, $F_{cn} = 1.00\times10^{2}$ and $q_{do} = 100\times e$ [1-5]. The dust-charge fluctuation time scale is taken as, $\tau_{cf} = (dq_d/q_d dt)^{-1} \sim q_{do}/I_o \sim 10^{-6}$ [25] for all the graphs. Since, we are interested in the fluctuation dynamics on the astrophysical scale, we take $\xi_e = 3\lambda_J$, and $\xi_i = 1.5\lambda_J$, where, $\lambda_J = 1.65\times10^{12}$ m. Here, λ_J is calculated for average interstellar mass density, $\rho_d = m_d n_d \sim 10^{-28}$ kg m^{-3}, and plasma temperature, $T_p \sim 1$ eV [1-5]. This unique transition in the potential profile (Figure 6.2(a)) is collectively due to the combined effect of decreasing m_d and n_{eo}; and increasing n_{dco} and n_{io}. The basic physics behind this transition is that increasing number density of the charged dust grains and ions increases the electrostatic repulsion between the Coulombic (charged) particles. But, the self-gravitational attraction decreases due to the decreasing grain mass. Thus, there is an unbalanced electro-gravitational periodic variation, which results in these types of transition of

eigenmodes. The damping nature of the wave amplitude increases as the oscillatory shock-like fluctuations propagate apart from the center ($\rho > 5\lambda_J$) of the cloud mass.

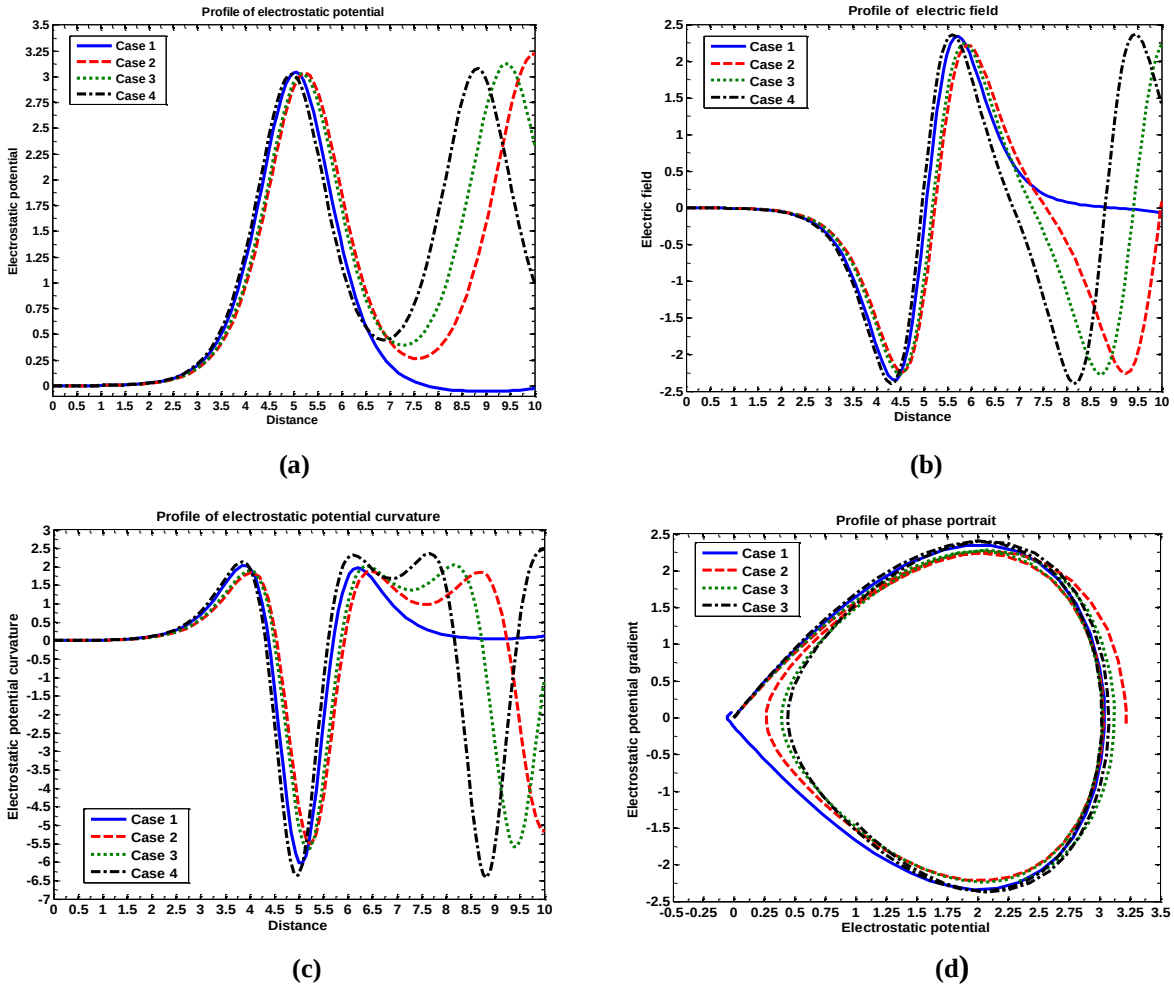

Figure 6.2 *Spatial profile of the normalized lowest-order perturbed (a) electrostatic potential showing a unique dynamical transition from soliton to oscillatory shock-like structure, (b) electric field, (c) potential curvature, and (d) phase portrait due to multi-parameter variation. Various lines correspond to Case (1):* $m_d = 7.00 \times 10^{-9}$ *kg,* $n_{dco} = 5.00 \times 10^{1}$ m^{-3}, $n_{eo} = 1.00 \times 10^{3}$ m^{-3}, *and* $n_{io} = 7.00 \times 10^{3}$ m^{-3} *(blue line), Case (2):* $m_d = 6.30 \times 10^{-9}$ *kg,* $n_{dco} = 7.33 \times 10^{1}$ m^{-3}, $n_{eo} = 6.60 \times 10^{2}$ m^{-3}, *and* $n_{io} = 7.50 \times 10^{3}$ m^{-3} *(red line), Case (3):* $m_d = 5.60 \times 10^{-9}$ *kg,* $n_{dco} = 9.66 \times 10^{1}$ m^{-3}, $n_{eo} = 3.30 \times 10^{2}$ m^{-3}, *and* $n_{io} = 8.00 \times 10^{3}$ m^{-3} *(green line), and Case (4):* $m_d = 4.90 \times 10^{-9}$ *kg,* $n_{dco} = 1.20 \times 10^{2}$ m^{-3}, $n_{eo} = 1.00 \times 10^{2}$ m^{-3}, *and* $n_{io} = 8.50 \times 10^{3}$ m^{-3} *(black line), respectively. Various input and initial parameter values are presented in the text.*

This may be due to decrease of the electro-gravitational coupling process. The physical strength of the potential fluctuation for normalized value ~ 1 is estimated as $\Phi_{phys} \sim \in \left(T_p \Phi_1 / e\right) \sim 10^{-2}$ V in the HII region with $\in = 10^{-2}$ [1-5]. Figure 6.2(b**)** graphically shows the field fluctuation with a transition from a mixture of compressive and rarefective soliton-like eigenmode to a chain-mixture of compressive and rarefective solitons. The real strength of the field fluctuation is $E_{phys} \sim \in \left(T_P E_{e1} / e\lambda_J\right) \sim 2.27 \times 10^{-14}$ V m^{-1}. Figure 6.2(c) gives the corresponding fluctuations in the plasma quasi-neutrality. It is seen that with the increasing n_{dco} and n_{io}; and decreasing n_{eo}, the strength of total charge is highly increased, which gives highly fluctuating quasi-neutrality. The lowest-order electrostatic potential curvature strength of the inhomogeneous DMC is calculated as $\left(\partial_{xx}\Phi\right)_{phys} \sim \in \left(T_p \partial_{\rho\rho} \Phi_1 / e\lambda_J^2\right) \sim 4.49 \times 10^{-26}$ V m^{-2}. The corresponding phase portraits (Figure 6.2(d)) show the geometrical trajectories with a transition from weakly conservative to non-conservative nature of the dynamics. It reveals that the system becomes highly non-conservative with the increasing n_{dco}, and n_{io}. The evolutionary profiles of the fluctuations supported in the cloud due to other sensitive plasma parameter variations are discussed in detail in Ref. [26].

For 3-D spatiotemporal analysis, equation (6.11) is simulated by finite-difference method. Figure 6.3(a) depicts the surface-profile of the normalized perturbed potential under the same condition as figure 6.2, but with $\left(M_{dco}\right)_i = 0.001\eta$, $\left(Q_{do}\right)_i = 0.01\eta$, and $\left(\Phi_1\right)_{\eta i} = 3.2 \sec h^2 \left\{1/2\left(\eta - 10\right)\right\}$. The boundary conditions applied here are (i) all the densities and dust-charge at infinity are asymptotically zero, (ii) all the velocities at the center of the cloud are zero, and (iii) all the potentials at the center and asymptotically at infinity are zero. Figure 6.3(b), similarly, shows the profile of normalized potential growing as oscillatory shock-like structure with $\left(\Phi_1\right)_{\eta i} = 2.5 \sec h^2 \left\{1/2\left(\eta - 10\right)\right\} + 0.03\eta^2$. Different input initial values used here are same as figure 6.2 but with $\left(M_{eo}\right)_i = 1.00 \times 10^{-1}$, $\left(\Phi_o\right)_i = -1.00 \times 10^{-3}$, $\left(\Phi_o\right)_{\rho i} = -1.00 \times 10^{-7}$, $\left(M_{io}\right)_i = 1.00 \times 10^{-2}$, $\left(M_{dco}\right)_i = 9.00 \times 10^{-3}$, $\left(\Psi_o\right)_{\rho i} = -7.00 \times 10^{-3}$, $\left(\Phi_1\right)_i = -9.10 \times 10^{-10}$, $\left(\Phi_1\right)_{\rho i} = -1.00 \times 10^{-6}$, $\left(\Phi_1\right)_{\rho\rho i} = 1.20 \times 10^{-4}$. Different parameters kept fixed are $n_{io} = 4.20 \times 10^3$ m^{-3}, $n_{dco} = 3.00 \times 10^1$ m^{-3}, $\mu = 1.80 \times 10^{-2}$, $F_{ed} = 1.79 \times 10^2$, and $F_{id} = 2.15 \times 10^2$ [1-5]. The strength of amplitude of the time-dependent surface plots evolving as soliton and shock-like structures is same as that of the time-independent profile (Figure 6.2(a)), which is $\Phi_{phys} \sim 10^{-2}$ V.

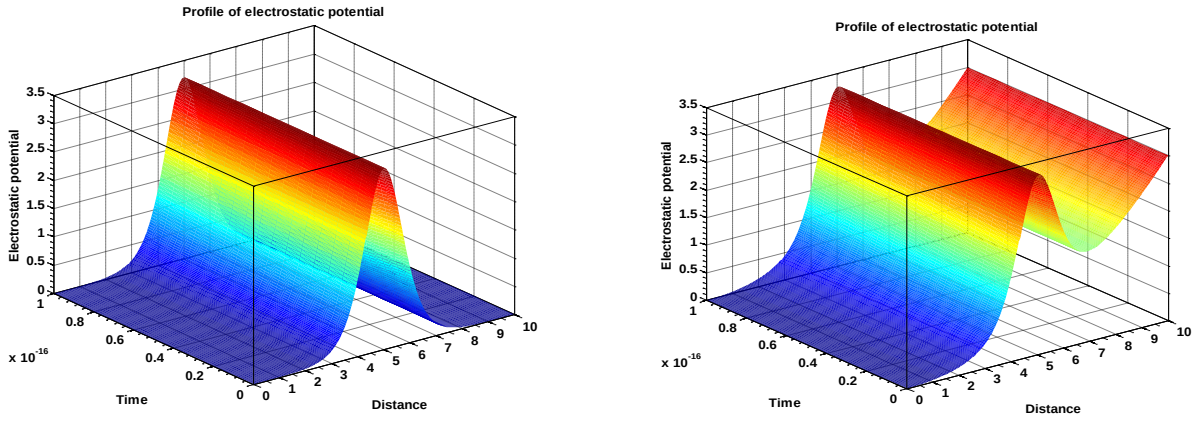

(a) **(b)**

Figure 6.3 *Spatiotemporal profile of the normalized lowest-order perturbed electrostatic potential evolving as (a) soliton-like structure, and (b) shock-like structure under the same condition as figure 6.2. The boundary conditions and input initial values are presented in the text.*

6.5.2 Self-gravitational Fluctuations

It is shown that the Jeans mode fluctuation dynamics is governed by the *d*-KdV equation on the lowest-order perturbed self-gravitational potential (Ψ_1) with a self-consistent linear source (equation (6.19)). The dynamics is contributed jointly by all the species having inertial mass. To obtain the detailed features, the system is simulated numerically as before. The resulting profiles are presented in figures 6.4-6.5. Figure 6.4 displays profile of the lowest-order perturbed self-gravitational (a) potential showing a unique transition from soliton to oscillatory shock-like eigenmode structure (blue, red, and green lines are rescaled by dividing with 2.50×10^{-2}, 7.52×10^{-2} and 2.78×10^{-1}, respectively), (b) field (blue, red, and green lines are rescaled by multiplying with 0.5×10^{2}, 0.18×10^{2} and 4.80, respectively), (c) potential curvature (blue, red, and green lines are rescaled by multiplying with 1.66×10^{2}, 7.07×10^{1}, and 1.26×10^{1}, respectively), and (d) phase portrait (blue, red and green lines are rescaled by multiplying with 4.09, 2.68, and 1.61, respectively) due to cloud multi-parameter variation. Various lines link to Case (1): $n_{io}=8.00\times10^{3}$ m^{-3}, $n_{dco}=2.40\times10^{-1}$ m^{-3}, $n_{dno}=4.30\times10^{1}$ m^{-3}, $F_{ed}=1.95\times10^{3}$, and $F_{id}=1.47\times10^{3}$ (blue line), Case (2): $n_{io}=7.57\times10^{3}$ m^{-3}, $n_{dco}=2.43\times10^{-1}$ m^{-3}, $n_{dno}=4.36\times10^{1}$ m^{-3}, $F_{ed}=1.9234\times10^{3}$, and $F_{id}=1.413\times10^{3}$ (red line), Case (3):

$n_{io} = 7.14 \times 10^3$ m^{-3}, $n_{dco} = 2.46 \times 10^{-1}$ m^{-3}, $n_{dno} = 4.43 \times 10^1$ m^{-3}, $F_{ed} = 1.8968 \times 10^3$, and $F_{id} = 1.3568 \times 10^3$ (green line); and Case (4): $n_{io} = 6.71 \times 10^3$ m^{-3}, $n_{dco} = 2.50 \times 10^{-1}$ m^{-3}, $n_{dno} = 4.50 \times 10^1$ m^{-3}, $F_{ed} = 1.87 \times 10^3$, and $F_{id} = 1.30 \times 10^3$ (black line), respectively. Different input initial values used $(N_{eo})_i = 1.00$, $(M_{eo})_i = 1.00 \times 10^{-2}$, $(\Phi_o)_i = -1.00 \times 10^{-3}$, $(\Phi_o)_{pi} = -1.00 \times 10^{-7}$, $(N_{eo})_i = 1.00$, $(M_{io})_i = 1.01 \times 10^{-2}$, $(N_{dco})_i = 1.00$, $(M_{dco})_i = 4.00 \times 10^{-4}$, $(M_{dno})_i = 1.00 \times 10^{-4}$, $(\Psi_o)_i = 2.00 \times 10^{-6}$, $(\Psi_o)_{pi} = -3.00 \times 10^{-10}$, $(Q_{do})_i = 1.00$, $(N_{dno})_i = 1.00$, $(\Psi_1)_i = -2.00 \times 10^{-5}$, $(\Psi_1)_{pi} = -4.00 \times 10^{-10}$, $(\Psi_1)_{ppi} = -1.00 \times 10^{-6}$. Different parameters kept fixed are $m_d = 7.00 \times 10^{-9}$ kg, $n_{eo} = 1.00 \times 10^3$ m^{-3}, $n_{io} = 8.00 \times 10^3$ m^{-3}, $n_{dco} = 2.40 \times 10^{-1}$ m^{-3}, $n_{dno} = 4.30 \times 10^1$ m^{-3}, $\mu = 5.00$, $F_{edc} = 10.01 \times 10^2$, $F_{idc} = 1.00 \times 10^2$, $F_{ed} = 1.95 \times 10^3$, $F_{id} = 1.47 \times 10^3$, $F_{cn} = 1.00 \times 10^2$ and $q_{do} = 96 \times e$ [1-5]. The unique transition from soliton to damped oscillatory shock-like eigenmode occurs due to collective effects resulting from increasing n_{do}; and decreasing n_{io}, F_{ed}, and F_{id}. The numerically found solitary structures arise due to the inhomogeneous balancing between nonlinear wave-breaking (due to fluidity) and linear dispersive effect (due to the self-gravity), where the wave-damping dissipative forces (due to the dust-charge fluctuation and collisions) are relatively weak. But, the shock-like eigenmodes develop due to the balance between nonlinearity and the combined influence of dispersive and dissipative forces. When the equilibrium Newtonian particle density increases, the dispersive effect becomes more dominant over the weak dissipative effect due to decreasing n_{io}, F_{ed}, and F_{id}. Thus, damped oscillatory shock-like eigenmodes with higher amplitudes results. The strength of the self-gravitational fluctuations is $\Psi_1 \sim 10^{-3}$, which is equivalent to $\left|\Psi_{phys}\right| \sim \in \left(T_p \Psi_1 / e\right) \sim 10^{-5}$ V. The corresponding field and curvature profiles are shown in figures 6.4(b)-6.4(c) with respective strength $\left|E_{gphys}\right| \sim \in \left(T_p E_{g1} / e\lambda_J\right) \sim 1.20 \times 10^{-15}$ V m^{-1} and $\left|\left(\partial_{xx}\Psi\right)_{phys}\right| \sim \in \left(T_p \partial_{\rho\rho} \Psi_1 / e\lambda_J^2\right) \sim 3.67 \times 10^{-30}$ V m^{-2}. The phase trajectories (Figure 6.4(d)) show a transition from nearly conservative system to highly non-conservative one due basically to the transition of closed-form to open oscillatory curved nature with rest of the features as discussed above. The self-gravitational fluctuation spectral patterns supported in the inhomogeneous DMC due to other sensitive plasma parameter variations under different realistic astrophysical conditions are elaborately discussed in Ref. [26].

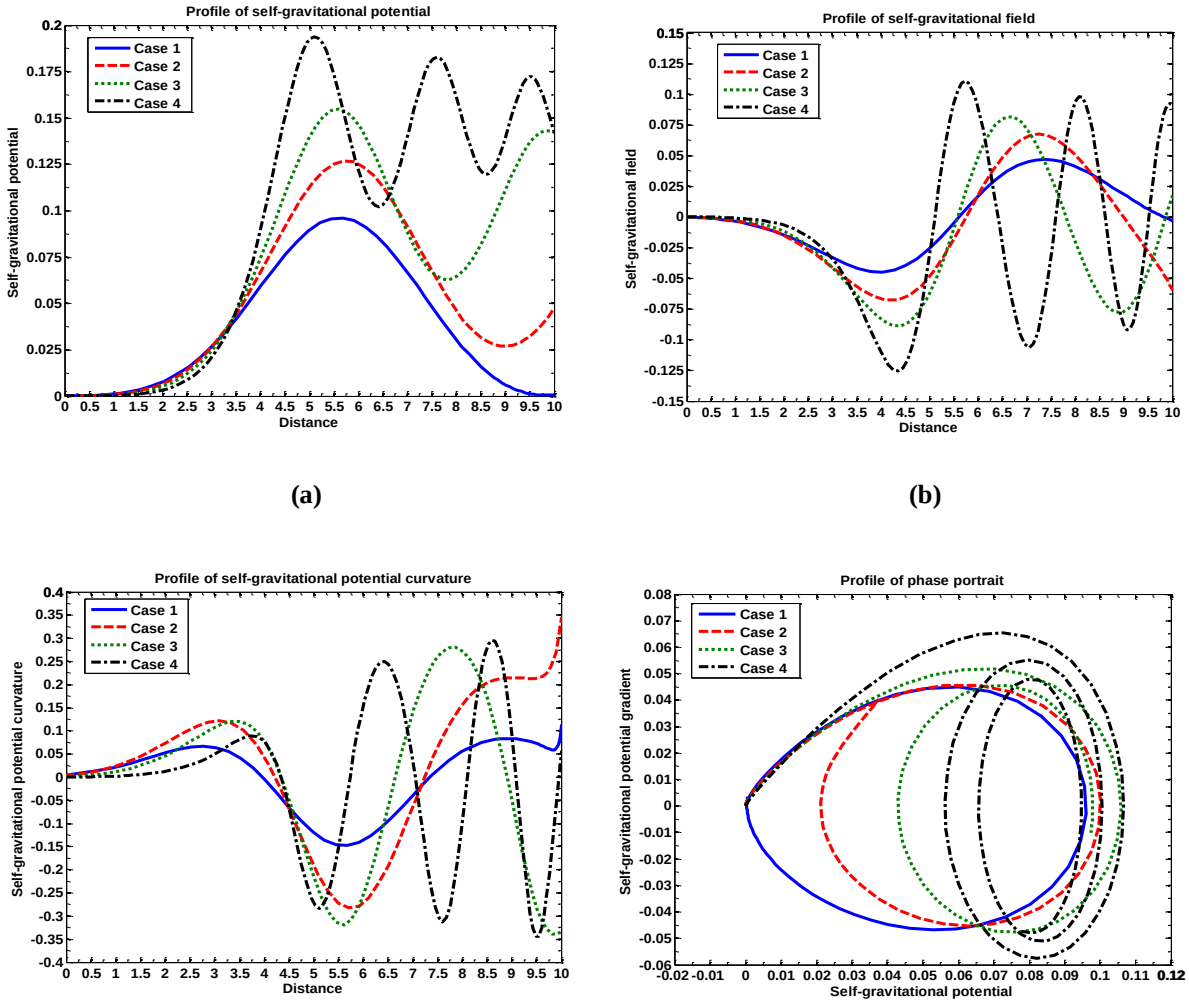

Figure 6.4 *Spatial profile of the normalized lowest-order perturbed self-gravitational (a) potential showing a unique characteristic transition from soliton to oscillatory shock-like eigenmode structure, (b) field, (c) potential curvature, and (d) phase portrait due to cloud multi-parameter variation. Various lines correspond to Case (1):* $n_{io} = 8.00 \times 10^{3}$ m^{-3}, $n_{dco} = 2.40 \times 10^{-1}$ m^{-3}, $n_{dno} = 4.30 \times 10^{1}$ m^{-3}, $F_{ed} = 1.95 \times 10^{3}$, *and* $F_{id} = 1.47 \times 10^{3}$ *(blue line), Case (2):* $n_{io} = 7.57 \times 10^{3}$ m^{-3}, $n_{dco} = 2.43 \times 10^{-1}$ m^{-3}, $n_{dno} = 4.36 \times 10^{1}$ m^{-3}, $F_{ed} = 1.9234 \times 10^{3}$, *and* $F_{id} = 1.413 \times 10^{3}$ *(red line), Case (3):* $n_{io} = 7.14 \times 10^{3}$ m^{-3}, $n_{dco} = 2.46 \times 10^{-1}$ m^{-3}, $n_{dno} = 4.43 \times 10^{1}$ m^{-3}, $F_{ed} = 1.8968 \times 10^{3}$, *and* $F_{id} = 1.3568 \times 10^{3}$ *(green line), and Case (4):* $n_{io} = 6.71 \times 10^{3}$ m^{-3}, $n_{dco} = 2.50 \times 10^{-1}$ m^{-3}, $n_{dno} = 4.50 \times 10^{1}$ m^{-3}, $F_{ed} = 1.87 \times 10^{3}$, *and* $F_{id} = 1.30 \times 10^{3}$ *(black line), respectively. Various input and initial parameter values are given in the text.*

To understand the spatiotemporal evolution of the fluctuations, equation (6.19) is numerically simulated by finite difference method as before. The 3-D surface plots thus obtained are shown in figure 6.5. Figure 6.5(a) depicts the profile of the self-gravitational potential as soliton-like structure under the same condition as figure 6.4, but with $(Q_{do})_i = 0.01\eta$, and $(\Phi_1)_{\eta i} = 1.6\times10^{-3}\,\mathrm{sec}h^2\{1/2(\eta-9.5)\}$. The choice of the initial inputs in all the cases is based on the fact that the steady-state evolution is now known, but the temporal evolution of which is yet to be known. The magnitude of this profile is same as that of the time-stationary ones (Figure 6.4(a)). Figure 6.5(b) shows the spatiotemporal growth profile of the potential shock-like structure with $(\Phi_1)_{\eta i} = sech^2\{1/2(\eta-10)\}+0.07\eta$. Different input initial values used here are same as figure 6.4, but with $(\Phi_o)_{\rho i} = -1.00\times10^{-4}$, $(M_{io})_i = 1.01\times10^{-3}$, $(M_{dno})_i = 5.00\times10^{-4}$, $(\Psi_o)_i = -1.00\times10^{-8}$, $(\Psi_o)_{\rho i} = -1.00\times10^{-9}$, $(\Psi_1)_i = -1.20\times10^{-8}$, $(\Psi_1)_{\rho i} = -4.00\times10^{-15}$, and $(\Psi_1)_{\rho\rho i} = 1.10\times10^{-10}$. Different parameters kept fixed are $m_d = 1.00\times10^{-9}$ kg, $n_{dno} = 3.70\times10^{1}$ m^{-3}, $F_{edc} = 1.10\times10^{2}$, $F_{ed} = 1.05\times10^{2}$, $F_{id} = 2.04\times10^{2}$, and $q_{do} = 132\times e$ [1-5]. The strength of amplitude of the time-dependent surface plots evolving as shock-like structure is $|\Psi_{phys}| \sim \in (T_p\Psi_1/e) \sim 10^{-2}$ V.

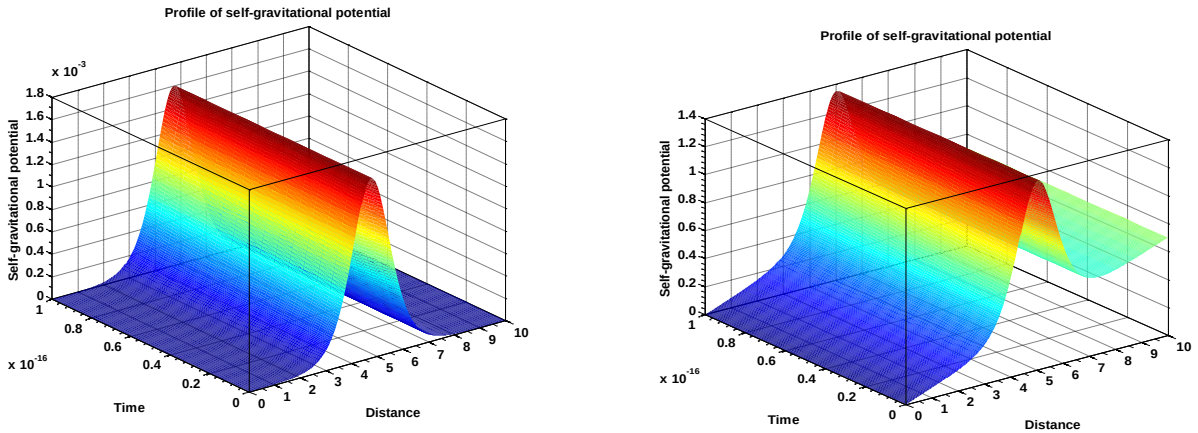

(a) **(b)**

Figure 6.5 *Spatiotemporal profile of the normalized lowest-order perturbed electrostatic potential evolving as (a) soliton-like structure, and (b) shock-like structure under the same condition as figure 6.4. The boundary conditions and input initial values are presented in the text.*

6.6 CONCLUSIONS

A simplified theoretical model to describe the properties of gravito-electrostatic fluctuation dynamics in an inhomogeneous, collisional, partially-ionized, self-gravitating cloud is proposed. All the possible realistic dynamical agencies of astrophysical scenario are taken into account. The lowest-order inertial correction of the thermal species is afresh included in the analysis. Unlike others in the past, a full spatiotemporal picture of the evolutionary equilibrium inhomogeneities is included in this model within the framework of planar geometry approximation. This is the unique originality of this articulation amidst all the realistic possible factors encountered by the different constituent species in hydrodynamic equilibrium configuration simultaneously. Standard non-local treatment is applied to derive a unique pair of self-gravitationally coupled *d*-KdV equations having self-consistent linear sources. By numerical analysis, it is inferred that both solitary and shock-like structures are supported in the cloud. A comprehensive spatiotemporal shape-analysis supports that such eigenmode structures indeed trigger the initial conditions in the formation processes of self-gravitationally bounded structures like stars and other planetary objects, which is in good agreement with others works. The main conclusive remarks are of astrophysical significance and the implication which may be proposed from the presented analysis are as follows.

(1) The lowest-order nonlinear gravito-electrostatic fluctuations of a planar inhomogeneous DMC amidst spatiotemporally inhomogeneous diverse equilibrium gradients are governed by a unique pair of coupled *d*-KdV equations.

(2) The electrostatic and self-gravitational potential fluctuations co-evolve as new soliton and damped oscillatory shock-like eigenmodes. Their structures are in good correspondence with the experimentally detected shocks and solitons in collision-dominated plasmas [3, 9], multispace satellite observations like Freja, Viking, etc. [3, 18-20], and earlier theoretical findings even based on local analyses by others [8, 10-11, 15].

(3) The eigenmode structures are contributed by the collective gravito-electrostatic dynamics of the inertial species and thermal species with weak but finite inertia amidst an integrated interplay of diverse nonlinear (hydrodynamic in origin), linear dispersive (deviation from quasi-neutrality and self-gravitational in origin through large-scale dynamics) and weakly dissipative (collisional and inhomogeneity in origin) effects.

(4) The effect of dust-charge variation on the propagation of gravito-electrostatic waves is of scientific importance for space and astrophysical contexts. The condensation of the grains due

to the propagation of the gravito-electrostatic shocks and solitons enhance the gravitational interaction, which is a feasible process for star formation through self-gravitational collapse mechanism as mentioned elsewhere [4, 12, 20-21].

(5) The explicit regions in the plasma parameter space are successfully found where unique shape-transitions from shock to soliton and vice versa exist in the multi-species molecular cloud. The corresponding fluctuations in field, curvature, scale-length and parametric trajectories are also elaborately analyzed. Our results on wave amplitude structures give theoretical supports to the earlier predictions *in situ* made by various spacecraft instrumentations, on-board multispace satellite reports, and experimental findings [3-4, 9, 18-19]. Examples of such clouds rich in like spectral patterns are *Lynds 204 Complex*, *Barnard 68*, and so forth. The methodological analysis may also be extensively applied to study the observed data on the dynamics of jets and associated bow shocks on the galactic scales as observed in certain galaxies like M51, NGC 1068, NGC 5258, Circinus, Mrk 673, and so forth [4, 19].

(6) The geometrical trajectories of the Columbic particles show that the system undergoes transition from weakly conservative to highly non-conservative one for the combined effect of decreasing dust-mass, equilibrium ion density and increasing electron and charged dust density. In contrast, the parametric trajectories depicting the geometric patterns of the Newtonian particles depict the self-gravitational dynamics transiting from conservative to highly non-conservative one for the combined effect of increasing dust densities and decreasing ion density, electron-dust and ion-dust collision frequencies in the cloud.

(7) It is equivalently found by comparing the electrostatic and self-gravitational fluctuations $\left(\left|\Phi_{phy}/\Psi_{phy}\right| \sim 10^{1}-10^{3}\right)$ that the electrostatic fluctuations are more dominant than the self-gravitational counterparts. Moreover, the inhomogeneous equilibrium admits dominant self-gravitational effects for $\left(Gm_d^2/q_d^2\right) \sim 1$ like in the HII region leading to bounded structure creation.

(8) This work puts a strong demonstration on the stability analyses of self-gravitating non-uniform medium without applying the Jeans homogenization assumption. It establishes that consideration of diverse equilibrium inhomogeneities gives a realistic picture of the fluctuation patterns, where the Jeans swindle application may be avoided.

(9) Our pulsational mode stability analysis based on the grainy Coulomb collisions in presence of grain-charge fluctuations, gravito-electrostatic equilibrium inhomogeneities and weak but finite inertia of the plasma thermal species may give rise to a new acceleration mechanism

called *charge-fluctuation-induced acceleration* (in hydrodynamic approach), or *Fermi acceleration* (in magnetohydrodynamic formalism) in astrophysical plasma and space environments [20]. This novel mechanism is likely to affect the rate of grain flow, coagulation and scattering of the population density of small grains (radius~$0.10\,\mu m$). As per the law of conservation of energy, the new energy sources for this kind of acceleration mechanism comes from the various irreversible plasma processes (triggered by the interaction of the electron-ion currents) occurring on the grain surfaces in the background plasma configuration. In presence of strong convective nonlinearity, the grain charge fluctuation via the grain-grain Coulombic interaction may result in higher-order accelerations applied to understand the dynamical evolution of the smallest grains to a regime beyond the Brownian motion [20].

(10) Finally, our study may broadly be useful as basic elements in investigating the basic features of the self-gravitational collapse, formation and evolution of stars, galactic structures and other cluster-like astrophysical objects in different practical regimes of interstellar space and plasma environments. The presented results may furthermore be helpful in understanding diverse astrophysical shocks with different characteristics, their effects in dissipating flow-energy, in heating astrophysical matter, in accelerating particles to high presumably cosmic-ray energies as mentioned above, and also in generating detectable electromagnetic radiation from radio to X-rays. This is because it is initially the dynamics of nonlinear disturbances, collective waves and oscillations in dusty clouds in interstellar medium which ultimately governs the dynamical formation mechanism of their gravito-electrostatically bounded structures ultimately in space and astrophysical situations.

REFERENCES

1. Spitzer, L., Jr. *Physical Processes in the Interstellar Medium*, WILEY-VCH Verlag GmbH & Co. KGaA, Weinheim, 2004.
2. Shukla, P. K. & Mamun, A. A. *Introduction to Dusty Plasma Physics*, IOP, Bristol and Philadelphia, 2002.
3. Verheest, F. Waves and instabilities in space plasmas, *Space Sci. Rev.* **77**, 267-302, 1996.
4. Vlahos, L. & Cargill, P. (eds.). *Turbulence in Space Plasmas*, Springer, Berlin Heidelberg, 2009.

5. Pandey, B. P., et al. The pulsational mode in the presence of dust charge fluctuations, *Phys. Scr.* **65**, 513-517, 2002.
6. Misra, A. P., et al. Electrostatic acoustic modes in a self-gravitating complex plasma with variable charge impurities, *Phys. Letts. A* **323**, 110-121, 2004.
7. Mamun, A. A. and Shukla, P. K. Electrostatic solitary and shock structures in dusty plasmas, *Phys. Scr.* **T98**, 107-114, 2002.
8. Xiao, D-L., et al. Evolution of nonlinear dust-ion-acoustic waves in an inhomogeneous plasma, *Phys. Plasmas* **13**, 052308(1)-052308(7), 2006.
9. Merlino, R. L., et al. Dusty plasmas: experiments on nonlinear dust acoustic waves, shocks and structures, *Plasma Phys. Control. Fusion* **54**, 124014(1)-(10), 2012.
10. Rao, N. N., et al. Dust-acoustic waves in dusty plasmas, *Planet. Space Sci.* **38**, 543-546, 1990.
11. Burman, S. and Chowdhury, A. R. Solitary waves in self-gravitating dusty plasma, *Chaos Sol. Fract.* **13**, 973-979, 2002.
12. Klessen, R. S., et al. Numerical star-formation studies-A status report, *Adv. Sci. Letts.* **4**, 258-285, 2011.
13. Mandal, G. and Tanisha, N. Y. Analysis of nonlinear dust-acoustic shock waves in an unmagnetized dusty plasma with q-nonextensive electrons where dust is arbitrarily charged fluid, *J. Appl. Math. Phys.* **3**, 103-110, 2015.
14. Mowafy, A. F. Propagation of dust ion acoustic waves in inhomogeneous warm dusty plasma, *African Review of Phys.* **7:0032**, 283-288, 2012.
15. Shukla, P. K. Low-frequency electromagnetic solitary and shock waves in an inhomogeneous dusty magnetoplasma, *Phys. Plasmas* **10**, 4907-4909, 2003.
16. Deka, U. and Dwivedi, C. B. Effect of electron inertial delay on Debye sheath formation, *Braz. J. Phys.* **40**, 333-339, 2010.
17. Asano, N. Wave propagation in non-uniform media, *Suppl. Prog. Theor. Phys*. **55**, 52-79, 1974.
18. Ergun, R. E., et al. FAST satellite observations of large-amplitude solitary structures, *Geophys. Res. Letts.* **25,** 2041-2044, 1998.
19. Watkins, R., et al. Nonlinear waves and solitons in molecular Clouds, in *The Physics and Chemistry of Interstellar Molecular Clouds*, Proceedings of the 2nd Cologne–Zermatt

Symposium Held at Zermatt. Switzerland, 21-24 September 1993, G. Winnewisser, & G. C. Pelz, eds., Springer, New York, 1995, 115-117.

20. Ivlev, A. V., et al. Acceleration of small astrophysical grains due to charge fluctuations, *Astrophys. J.* **723,** 612-619, 2010.
21. Chiuderi, C. & Velli, M. *Physics of Plasma Astrophysics*, Springer-Verlag, Italia, 2015.
22. Cadez, V. M. Applicability problem of Jeans criterion to a stationary self-gravitating cloud, *Astron. Astrophys.* **235**, 242-244, 1990.
23. Misra, A. P., et al. Acoustic waves in a self-gravitating collisional dusty plasma, *Phys. Scr*. **71** 207-212, 2005.
24. Otto, S. R. & Denier, J. P. An *Introduction to Programming and Numerical Methods in MATLAB*, Springer, London, 2005.
25. Ma, J. X. and Liu, J. Dust acoustic soliton in a dusty plasma, *Phys. Plasmas* **4**, 253-255, 1997.
26. Borah, B. and Karmakar, P. K. Nonlinear waves in a self-gravitating charge varying collisional dust molecular cloud in presence of diverse equilibrium inhomogeneities, *Phys. Scr*. **89**, 125602(1)-125602(26), 2014.